NANO LETTERS

2008
Vol. 8, No. 3
945-949

Silicon Nanoribbons for Electrical Detection of Biomolecules

Niklas Elfström,*,† Amelie Eriksson Karlström,‡ and Jan Linnros†

Department of Microelectronics and Applied Physics, Royal Institute of Technology, SE-164 40 Stockholm, Sweden, and Department of Biotechnology, Royal Institute of Technology, SE-106 91 Stockholm, Sweden

Received January 11, 2008

ABSTRACT

Direct electrical detection of biomolecules at high sensitivity has recently been demonstrated using semiconductor nanowires. Here we demonstrate that semiconductor nanoribbons, in this case, a thin sheet of silicon on an oxidized silicon substrate, can approach the same sensitivity extending below the picomolar concentration regime in the biotin/streptavidin case. This corresponds to less than ~20 analyte molecules bound to receptors on the nanoribbon surface. The micrometer-size lateral dimensions of the nanoribbon enable optical lithography to be used, resulting in a simple and high-yield fabrication process. Electrical characterization of the nanoribbons is complemented by computer simulations showing enhanced sensitivity for thin ribbons. Finally, we demonstrate that the device can be operated both in inversion as well as in accumulation mode and the measured differences in detection sensitivity are explained in terms of the distance between the channel and the receptor coated surface with respect to the Debye screening length. The nanoribbon approach opens up for large scale CMOS fabrication of highly sensitive biomolecule sensor chips for potential use in medicine and biotechnology.

Semiconducting nanowires have been shown to have potential use in label-free, high-sensitivity, direct electrical detection of biomolecules.[1–8] The high detection sensitivity can be attributed to their small size, enabling local charge transfers, such as when analyte molecules bind to receptor molecules at the surface of the nanowire, to result in a current change due to a field effect. This effect is sufficiently strong that, in principle, single charges at the surface of the nanowire[9,10] can be sensed. The nanowires operate similarly as field-effect transistors where, indeed, single charge carrier effects have been demonstrated even at room temperature[11] for channel dimensions in the sub-50 nm range.

Fabrication of semiconductor nanowires is, however, complicated, involving either top-down approaches[2,7,12,13] using advanced lithography or bottom-up growth techniques.[1,5,6,14,15] Here, we present a scheme where the precise lateral definition is relaxed using a "nanoribbon" approach where a thin sheet of silicon replaces the nanowire, the surface of which is coated by suitable receptor molecules to enable biomolecule detection. We demonstrate the technique by fabricating nanoribbons of different thicknesses and measuring their response for a model receptor/analyte system. The sensitivity is below the picomolar concentration regime, corresponding to less than 20 analyte molecules bound to the nanoribbon, and approaches or equals therefore that of nanowires.

When analyzing possible detection limits for biomolecule sensing for nanowires versus nanoribbons, one may note that the sensitivity increases approximately as the surface to volume ratio of the channel,[7–9,13] although more sophisticated device simulation tools must be used for true quantitative modeling.[9,13,16] For detecting the binding of specific analyte biomolecules to their corresponding receptors immobilized on the surface of the channel, however, the situation is more complicated. Here, one must consider the total amount of analyte molecules in the solution with respect to available binding sites on the sensing surface and on other functionalized surfaces as well as the affinity of the binding reaction (and of any competing nonspecific binding). Indeed, in the limit of very low analyte concentrations, the fractional occupancy of receptors by analyte molecules increases as the available area for binding decreases (assuming constant receptor areal density).[17] In practice, however, it is difficult to restrict receptor immobilization to submicrometer dimensions and the total receptor area will, together with other parameters as stated above, determine the fractional occupancy of receptors. In such a case, a wide channel (nanoribbon) would simply bind proportionately more analyte molecules than a narrow (nanowire). The real critical parameter is instead the channel depth from the surface,

* Corresponding author. E-mail: niklasel@kth.se.
† Department of Microelectronics and Applied Physics, Royal Institute of Technology.
‡ Department of Biotechnology, Royal Institute of Technology.

10.1021/nl080094r CCC: $40.75
Published on Web 02/12/2008

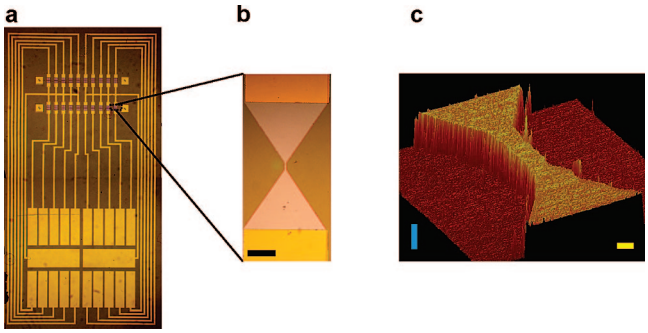

Figure 1. (a) Optical micrograph of the Si nanoribbon chip, in top view, showing the gold contact leads connecting to the Si microstructures that provide leads to the interior nanoribbon structure. (b) Top view optical micrograph of gold contacts connecting to the Si pads that lead to the nanoribbon (at centre). Length scale bar = 8 μm. (c) AFM topographical image of a 45 nm thick nanoribbon. Height scale bar (blue) = 50 nm. Length scale bar (yellow) = 1 μm.

which needs to be smaller than any screening length, being the combination of screening from ions in the solution and carriers in the semiconductor.

Silicon (Si) nanoribbons were fabricated from SOI material having an initial 340 nm thick top Si layer (p-doped ρ = 14–22 Ω cm). Using dry oxidation at 900 °C, the initial Si layer on three wafers was thinned down to thicknesses of 105, 65, and 50 nm as measured by AFM. The ~1 μm wide and ~2 μm long Si nanoribbons and Si contact leads were then defined using optical lithography and lift-off. The nanoribbons were subsequently oxidized at 900° for 15 min in an oxygen ambient, creating a ~5 nm thick SiO_2 layer. This oxide stabilizes the nanoribbon surface and prevents short-circuiting as the liquid is added. The oxide also creates a better surface for the following biomodification. Note also that the thinnest Si thickness is well above the critical value for the mobility not to change.[18] Figure 1a shows an optical micrograph of the nanoribbon chip, and Figure 1b shows an optical micrograph close up of a single nanoribbon. Figure 1c shows an atomic force microscopy (AFM) topographical image, indicating a uniform Si layer of ~50 nm thickness. Using a second optical lithography step, a TiW/Au metal layer 20/200 nm thick was added to the Si contact leads after a short HF dip removing the protective SiO_2 layer. The Si nanowire (point in Figure 4d) was created from a 105 nm thin SOI wafer using e-beam lithography. The Si contact leads were created using optical lithography aligning the Si contact leads with the nanowire. A protective oxide and metallization using the same parameters as for the nanoribbons finalized the nanowire device. For electrical characterization, a Keithley picoammeter (6487) and a KPCI-3201 D/A–A/D card was used. The I_{DS} – V_{DS} characteristics were obtained by sweeping the drain source voltage, keeping the back gate at a constant integer value.

From the device characteristics, displayed in Figure 2a−c, the nanoribbons show similar behavior as a Schottky barrier, metal oxide semiconductor field effect transistor (SBMOSFET). The conduction mechanism is through electrons in an inversion layer for positive back gate (substrate) bias, V_{GS}

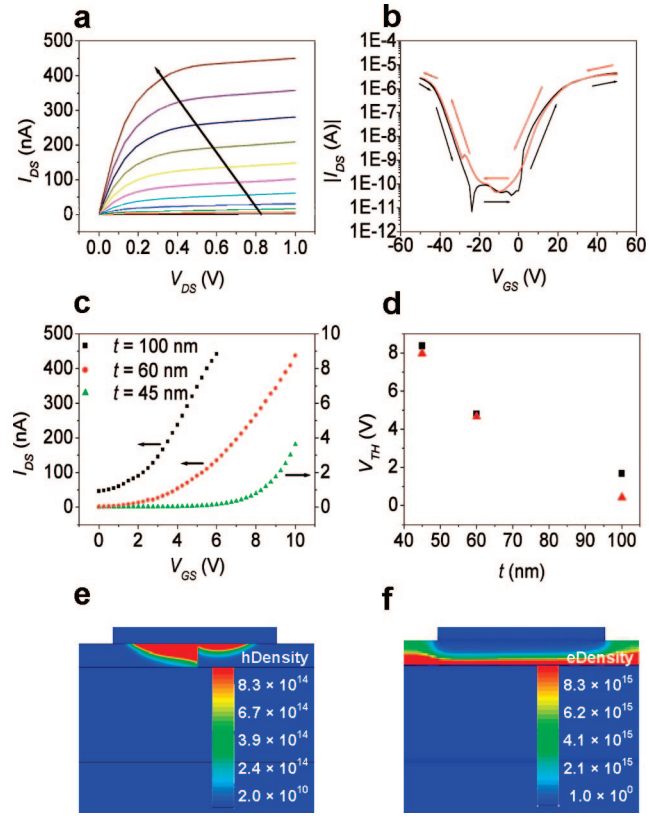

Figure 2. (a) I_{DS}–V_{DS} characteristics for a nanoribbon device of 60 nm thickness for V_{GS} = 0−10 V with a stepsize of 1 V. (b) Subthreshold plot for a nanoribbon of 45 nm thickness showing an ambipolar behavior. (c) I_{DS}–V_{GS} as obtained from the I_{DS}–V_{DS} characteristics at V_{DS} = 0.74 V for three nanoribbons of different thickness. For left axis: t = 100 nm (black squares) and 60 nm (red dots); for right axis: t = 40 nm (green triangles). (d) Threshold voltage extrapolated from the I_{DS}–V_{GS} characteristics in (c) plotted vs thickness (black squares). Red triangles show simulated threshold voltage for the same thicknesses. (e) Simulated hole density for a 100 nm thick nanoribbon at V_{DS} = 2 V and V_{GS} = −6 V, showing that the accumulation hole current runs at the top of the channel. (f) Simulated electron density for a 100 nm thick nanoribbon at V_{DS} = 2 V and V_{GS} = 6 V, showing that the inversion electron current runs at the bottom of the channel.

(similar to a n-channel MOSFET), and through holes in accumulation mode for negative back gate bias in a similar way as for Si nanowires.[16,19,20] In Figure 2b, the drain source current, I_{DS}, is plotted vs different back gate voltages, showing that the device is, indeed, ambipolar, also exhibiting hole conduction at large negative bias.[16] In Figure 2c, the I_{DS}−V_{GS} characteristics is plotted at V_{DS} = 0.74 V. This shows that the threshold voltage is different for different thicknesses and the extrapolated[21] V_{TH} are further plotted in Figure 2d, yielding an inverse thickness dependence. We have previously shown that surface charges can have a huge impact on the conduction on Si nanowires.[9,12] These charges most likely stem from the fabrication process (presumably negative surface or interface states),[22,23] affecting the conduction mechanism and thereby the threshold voltage. The closer the surface charges are to the conducting channel, the larger the impact on it becomes and, therefore, the thinnest nanoribbon is more heavily affected by these charges. This is an early indication that thin nanoribbons can be used in

biosensor applications in a similar way as nanowires and that the sensitivity increases with decreasing thickness of the top Si layer.

To confirm the influence of channel thickness on threshold voltage, a computer simulation was performed for a cross section along the nanoribbon device using a two-dimensional semiconductor simulation package (ISE-TCAD). The charge between the lower silicon/silicon dioxide interface was set to a typical[22] value of $+1 \times 10^{11}$ cm^{-2}, while the charge at the upper interface was used to fit the simulated threshold voltage to that experimentally obtained. The best fit occurred for an interface charge of -5×10^{11} cm^{-2} (red triangles in Figure 2d). Figure 2f shows a corresponding electron density map revealing that the conducting electron channel is located at the bottom of the top Si layer. On the other hand, at large negative back gate voltages, the accumulation regime is entered and a hole channel forms at the top close to the surface, see Figure 2e.

Charged species binding to the nanoribbon surface will affect the electron current, but the distance over which this interaction can occur is set by the Debye length, λ_D, given by[21]

$$\lambda_D = \sqrt{\frac{\varepsilon_S k_B T}{q^2 N_B}}$$

where ε_S, k_B, T and q stand for permittivity, Boltzmann's constant, temperature, and charge quantum, respectively. In a bulk semiconductor, N_B would be the doping density, but in a highly inverted channel, the electron charge density would be more appropriate and we use the value 1×10^{16} cm^{-3} as obtained from the simulation (Figure 2f). This yields $\lambda_D = 40$ nm at room temperature, and we conclude that channel thickness must be in this range to reach a high surface charge sensitivity, important for biomolecule sensing.

The biomolecule sensing properties of the nanoribbon devices were tested using the well-known strong binding between biotin and streptavidin. After oxygen plasma etching, the surfaces of the Si nanoribbons and nanowires were aminofunctionalized with 3-aminopropyltriethoxysilane (APTES) in ethanol, after which the surface was rinsed with ethanol and deionized water. The biotinylation reagent NHS-PEO_{12}-biotin (Pierce) was then reacted with the surface-exposed amino groups in PBS, pH 7.4, for 30 min. Before biotinylation, the surface of the chip was coated with a polymer (acetyl acetate) except for the area where the nanoribbons were defined. On top of this area, a plastic container was placed to hold the aqueous solutions. For the binding experiments, stock solutions of streptavidin (Pierce) and human serum albumin (KabiVitrum) at concentrations ranging from 1×10^{-13} to 1×10^{-7} M in 0.1 × PBS, pH 7.4, were prepared. All binding experiments were performed in 0.1 × PBS, pH 7.4.

Streptavidin molecules binding to biotin molecules, immobilized on the nanoribbon surface, would affect the electron density in the nanoribbon channel due to their negative net charge,[24] resulting in a decrease of the current. Figure 3 shows a schematic for the experimental setup used in these experiments. The relatively large volume used

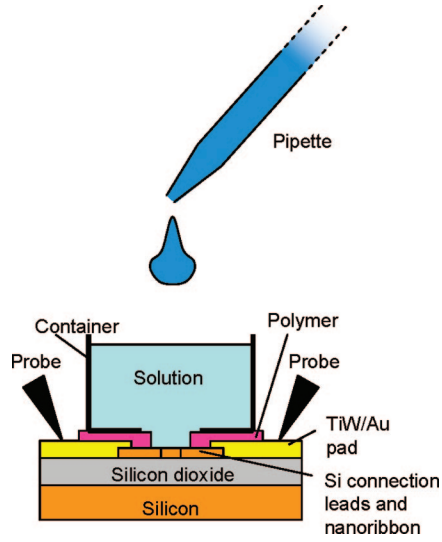

Figure 3. A polymer layer protects the gold contact leads and the Si microstructures connecting to the nanoribbon from shortcuts and leakage currents during the experiments. Tungsten probe needles connect to the gold contact pads. The plastic container glued on to the nanoribbon chip has a drilled hole ~2 mm × 2 mm in size in order for the solution to be in contact with the nanoribbon.

increases the time of binding (normally ~1000 s to reach equilibrium) due to mass transport limitations but creates more stable conditions for electrical measurements. In the experiments, 100 μL of 0.1× phosphate buffered saline (PBS) solution was initially added to the container (Figure 3) after surface functionalization with biotin. The salt concentration was kept at a low level to reduce Debye screening effects,[25] yielding $\lambda_D \sim 2.3$ nm (notably smaller than the electrical screening by channel electrons). The drain source current, I_{DS}, was then logged at $V_{DS} = 2.0$ V,[26] while a streptavidin solution of a specific concentration was added. Figure 4a shows the binding response of a 45 nm thick nanoribbon after addition of streptavidin to a final concentration of 6×10^{-13} M and to 1×10^{-9} M, respectively. Control experiments performed show that there is no reaction when human serum albumin, as a control protein, is instead added at the same concentration as streptavidin. A second control experiment was also performed where the nanoribbons were functionalized with APTES, but without biotinylation, showing no reaction upon addition of streptavidin.

The lowest detectable concentration corresponds to ~4×10^7 streptavidin molecules in the solution volume. Assuming that streptavidin binds uniformly to the functionalized Si surface open to the solution, the fraction of molecules binding to the nanoribbon surface amounts to only ~20 streptavidin molecules. This would be an upper limit, assuming that all streptavidin molecules in the solution bind to the biotinylated surface.

The binding response to different streptavidin concentrations was investigated for a nanoribbon of 45 nm thickness and is shown in Figure 4b. The curve shows that the response increases with increasing concentrations of streptavidin,[27] providing strong evidence that the current is specifically affected by the binding interaction. From the saturation at a concentration of ~1×10^{-9} M, we may calculate the areal

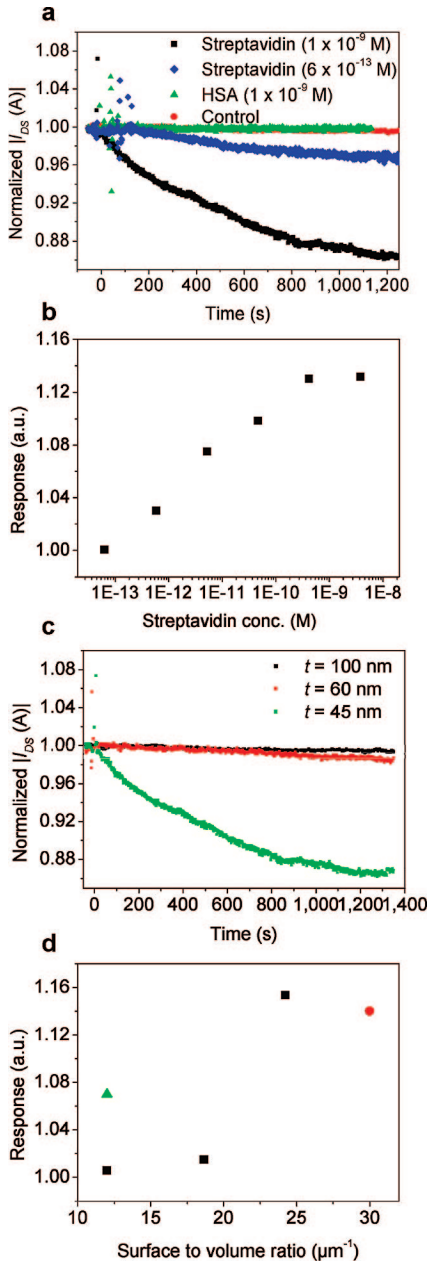

Figure 4. Addition of the solution occurs at time = 0 s in all experiments. (a) Normalized $|I_{DS}|$ upon detection of a 1×10^{-9} M (black squares) and a 6×10^{-13} M (blue diamonds) streptavidin solution. Included in the plot are also two control experiments for the addition of a 1×10^{-9} M human serum albumin (HSA) protein solution (red circles) and upon addition of a 1×10^{-9} M streptavidin solution to nonbiotinylated nanoribbons (control) (green triangles). (b) Response vs concentration plot for a nanoribbon of 45 nm thickness. The response is calculated as the ratio between the measured stable current when equilibrium has been reached after addition of streptavidin solution, I_1, and the measured stable current before addition of the streptavidin solution, I_0. (c) Normalized $|I_{DS}|$ upon detection of a 1×10^{-9} M streptavidin solution for different nanoribbon thicknesses, t. (d) Response, calculated as described above, vs surface to volume ratio for different nanoribbons, $t = 100$, 60, and 45 nm (black squares) and a nanowire $t = 100$ nm and $w = 100$ nm (red dot). Included in the plot is also the response (green triangle) for a nanoribbon of 100 nm thickness, run in accumulation mode for $V_{GS} = -30$ V, showing an increased response.

density of bound streptavidin molecules as 1.7×10^{12} cm^{-2} (again an upper limit assuming all moleules are bound to the open biotin coated surface). This corresponds to an average separation of ~8 nm, a reasonable value for close packing of proteins at a surface.

The response for different nanoribbon thicknesses is shown by the data in Figure 4c. Indeed, only the thinnest nanoribbon gives a strong response and we attribute this to Debye screening for the thicker nanoribbons. Extracting the asymptotic response, the data is replotted in Figure 4d vs surface to volume ratio. In accumulation mode, on the other hand, a hole channel forms close to the surface (Figure 2e) and the response would be enhanced. As a result, a good signal is observed even for a 100 nm thick ribbon (green triangle) as plotted in Figure 4d. Although in this case, data is much more noisy and unstable, so far for unknown reasons, and we have not been able to reach the same sensitivity as for the inverted channel. Included in the plot is also the response of a nanowire (red dot) fabricated using e-beam lithography.[9] Even though nanowires can be made at smaller dimensions, this clearly shows that Si nanoribbons can be made as sensitive as Si nanowires. In addition, it has previously been shown that the liquid volume and diffusion times for the ligand to reach the surface often sets a practical limit for nanoscale biosensors and that it becomes difficult to reach sensitivities significantly below the picomolar range[28] on a relevant time scale. Therefore, the much larger surface area of the nanoribbon may be a clear advantage in a biosensor application as diffusion time is reduced. The larger number of bound analytes most likely also improves measurement stability.

Summarizing, we have demonstrated that semiconductor nanoribbons, where thickness is on a few nanometer scale while lateral dimensions are on the micrometer scale, can be used as highly specific sensors for biomolecules with sensitivities approaching those of nanowires, i.e., in the subpicomolar concentration regime. We have also demonstrated sensing in the accumulation mode and pointed out important differences in the channel location, which together with Debye screening sets the ultimate sensitivity. The nanoribbon approach simplifies the fabrication process largely compared to the complicated schemes for nanowire fabrication such that even low-resolution CMOS technology can readily be used. This, together with the fact that SOI wafers with a uniform and thin Si layer nowadays are commercially available, shows that the nanoribbon is a good candidate for use as a highly sensitive biosensor. We foresee a large number of applications where label-free, direct electrical detection (e.g., in hand-held instruments) combined with cheap mass fabrication (enabling disposable chip use) is a clear advantage.

Acknowledgment. We thank Dr. R. Juhasz for introducing N.E. to Si chip biofunctionalization techniques and fruitful discussions during experiment design and manuscript preparation. This work was supported by the National Swedish Research Council (VR).

References

(1) Cui, Y.; Wei, Q.; Park, H.; Lieber, C. M. *Science* **2001**, *293*, 1289–1292.

(2) Li, Z.; Chen, Y.; Li, X.; Kamins, T. I.; Nauka, K.; Williams, R. S. *Nano Lett.* **2004**, *4*, 245–247.
(3) Fan, Z.; Lu, J. G. *Appl. Phys. Lett.* **2005**, *86*, 123510.
(4) Chen, R. J.; Choi, H. C.; Bangsaruntip, S.; Yenilmez, E.; Xiaowu, T.; Wang, Q.; Chang, Y.-L.; Dai, H. *J. Am. Chem. Soc.* **2004**, *126*, 1563–1568.
(5) Kamins, T. I.; Sharma, S.; Yasseri, A. A.; Li, Z.; Straznicky, J. *Nanotechnology* **2006**, *17*, S291–S297.
(6) Shao, M.-W.; Shan, Y.-Y.; Wong, N.-B.; Lee, S.-T. *Adv. Funct. Mater.* **2005**, *15*, 1478–1482.
(7) Stern, E.; Klemic, J. F.; Routenberg, D. A.; Wyrembak, P. N.; Turner-Evans, D. B.; Hamilton, A. D.; LaVan, D. A.; Fahmy, T. M.; Reed, M. A. *Nature* **2007**, *445*, 541–544.
(8) Fan, Z.; Lu, J. G. *IEEE Trans. Nanotechnol.* **2006**, *5*, 393–396.
(9) Elfström, N.; Juhasz, R.; Sychugov, I.; Engfeldt, T.; Eriksson Karlström, A.; Linnros, J. *Nano Lett.* **2007**, *7*, 2608–2612.
(10) Patolsky, F.; Zheng, G.; Hayden, O.; Lakadamyali, M.; Zhuang, X.; Lieber, C. M. *Proc. Natl. Acad. Sci. U.S.A.* **2004**, *101*, 14017–14022.
(11) Guo, L.; Leobandung, E.; Chou, S. Y. *Appl. Phys. Lett.* **1997**, *70*, 850–852.
(12) Juhassz, R.; Elfström, N.; Linnros, J. *Nano Lett.* **2005**, *5*, 275–280.
(13) Li, Z.; Rajendran, B.; Kamins, T. I.; Li, X.; Chen, Y.; Stanley Williams, R. *Appl. Phys. A: Mater. Sci. Process.* **2005**, *80*, 1257–1263.
(14) Shan, Y.; Kaan Kalkan, A.; Peng, C.-Y.; Fonash, S. J. *Nano Lett.* **2004**, *4*, 2085–2089.
(15) Whang, D.; Jin, S.; Wu, Y.; Lieber, C. M. *Nano Lett.* **2003**, *3*, 1255–1259.
(16) Koo, S.-M.; Edelstein, M. D.; Li, Q.; Richter, C. A.; Vogel, E. M. *Nanotechnology* **2005**, *16*, 1482–1485.
(17) Ekins, R. P. *Clin. Chem.* **1998**, *44*, 2015–2030.
(18) Choi, J.-H.; Park, Y.-J.; Min, H.-S. *IEEE Electron Device Lett.* **1995**, *16*, 527–529.
(19) Cui, Y.; Duan, X.; Hu, J.; Lieber, C. M. *J. Phys. Chem. B* **2000**, *104*, 5213–5216.
(20) Koo, S.-M.; Fujiwara, A.; Han, J.-P.; Vogel, E. M.; Richter, C. A.; Bonevich, J. E. *Nano Lett.* **2004**, *4*, 2197–2201.
(21) Sze, S. M. *Physics of Semiconductor Devices*, 2nd ed; John Wiley & Sons: New York, 1981.
(22) Seo, K.-I.; Sharma, S.; Yasseri, A. A.; Stewart, D. R.; Kamins, T. I. *Electrochem. Solid-State Lett.* **2006**, *9*, G69–G72.
(23) Kimukin, I.; Islam, M. S.; Stanley Williams, R. *Nanotechnology* **2006**, *17*, S240–S245.
(24) Ebner, A.; Kienberger, F.; Kda, G.; Stroh, C. M.; Geretschläger, M.; Kamruzzahan, A. S. M.; Wildling, L.; Travis Johnson, W.; Ashcroft, B.; Nelson, J.; Lindsay, S. M.; Gruber, H. J.; Hinterdorfer, P. *ChemPhysChem* **2005**, *6*, 897–900.
(25) Stern, E.; Wagner, R.; Sigworth, F. J.; Breaker, R.; Fahmy, T. M.; Reed, M. A. *Nano Lett.* **2007**, *7*, 3405–3409.
(26) Elfström, N.; Linnros, J. *Appl. Phys. Lett.* **2007**, *91*, 103502.
(27) Creighton, T. E. *Proteins - Structures and Molecular Properties*, 2nd ed.; W. H. Freeman and Company: New York, 1993.
(28) Sheehan, P. E.; Whitman, L. J. *Nano Lett.* **2005**, *5*, 803–807.

NL080094R